



Article

Using Remote Sensing to Estimate Understorey Biomass in Semi-Arid Woodlands of South-Eastern Australia

Linda Riquelme * , David H. Duncan , Libby Rumpff and Peter Anton Vesk

School of Ecosystem and Forest Sciences, The University of Melbourne, Parkville, VIC 3010, Australia; david.duncan@unimelb.edu.au (D.H.D.); lrumpff@unimelb.edu.au (L.R.); pvesk@unimelb.edu.au (P.A.V.)

* Correspondence: lriquelme@student.unimelb.edu.au

Abstract: Monitoring ground layer biomass, and therefore forage availability, is important for managing large, vertebrate herbivore populations for conservation. Remote sensing allows for frequent observations over broad spatial scales, capturing changes in biomass over the landscape and through time. In this study, we explored different satellite-derived vegetation indices (VIs) for their utility in estimating understorey biomass in semi-arid woodlands of south-eastern Australia. Relationships between VIs and understorey biomass data have not been established in these particular semi-arid communities. Managers want to use forage availability to inform cull targets for western grey kangaroos (*Macropus fuliginosus*), to minimise the risk that browsing poses to regeneration in threatened woodland communities when grass biomass is low. We attempted to develop relationships between VIs and understorey biomass data collected over seven seasons across open and wooded vegetation types. Generalised Linear Mixed Models (GLMMs) were used to describe relationships between understorey biomass and VIs. Total understorey biomass (live and dead, all growth forms) was best described using the Tasselled Cap (TC) greenness index. The combined TC brightness and Modified Soil Adjusted Vegetation Index (MSAVI) ranked best for live understorey biomass (all growth forms), and grass (live and dead) biomass was best described by a combination of TC brightness and greenness indices. Models performed best for grass biomass, explaining 70% of variation in external validation when predicting to the same sites in a new season. However, we found empirical relationships were not transferrable to data collected from new sites. Including other variables (soil moisture, tree cover, and dominant understorey growth form) improved model performance when predicting to new sites. Anticipating a drop in forage availability is critical for the management of grazing pressure for woodland regeneration, however, predicting understorey biomass through space and time is a challenge. Whilst remotely sensed VIs are promising as an easily-available source of vegetation information, additional landscape-scale data are required before they can be considered a cost-efficient method of understorey biomass estimation in this semi-arid landscape.

Keywords: aboveground biomass; forage; monitoring; Landsat; spectral indices; grazing management; ecological restoration and conservation; rangelands



Citation: Riquelme, L.; Duncan, D.H.; Rumpff, L.; Vesk, P.A. Using Remote Sensing to Estimate Understorey Biomass in Semi-Arid Woodlands of South-Eastern Australia. *Remote Sens.* **2022**, *14*, 2358. <https://doi.org/10.3390/rs14102358>

Academic Editors: Todd Robinson and Paul Nevill

Received: 30 March 2022

Accepted: 9 May 2022

Published: 13 May 2022

Publisher's Note: MDPI stays neutral with regard to jurisdictional claims in published maps and institutional affiliations.



Copyright: © 2022 by the authors. Licensee MDPI, Basel, Switzerland. This article is an open access article distributed under the terms and conditions of the Creative Commons Attribution (CC BY) license (<https://creativecommons.org/licenses/by/4.0/>).

1. Introduction

Monitoring aboveground biomass over broad spatial scales and frequent temporal intervals is essential in a range of fields, such as fuel mapping for fire management [1], monitoring ecosystem change [2,3], estimating agricultural yield [4], carbon accounting [5], and for quantifying forage for livestock production [6,7]. In the field of ecological conservation and restoration, optical remote sensing has been used to estimate forage availability for large vertebrate herbivore management in a range of environments (e.g., [8–12]).

Multispectral remote sensing of aboveground biomass typically employs the red and near infrared (NIR) bands, as these contain approximately 90% of vegetation information [13]. Chlorophyll absorbs visible radiation in the red wavelengths, whereas radiation

in the NIR wavelengths is reflected by leaf cellular structures [14]. Short-wave infrared (SWIR) bands are also sensitive to variations in vegetation, particularly water content [15]. Many vegetation indices (VIs) exist, using combinations of these bands to measure vegetation parameters, such as cover, standing biomass, and primary productivity [14,16]. Perhaps the most widely-used is the Normalised Difference Vegetation Index (NDVI), a simple ratio-based index sensitive to variation in red-NIR reflectance, and hence vegetation greenness and density [9,17].

Extending empirical relationships between field biomass and remote sensing data across space and time has often been challenging [18], though few studies have assessed this (e.g., [19–22]). The spectral response of vegetation may be affected by many factors such as canopy background (e.g., soil brightness and colour), vegetation and soil moisture, senescent vegetation and litter, and species composition [18,23,24]. As well as environmental factors, atmospheric effects can also contribute to signal noise [25]. As these factors can vary across different environments, many VIs have been developed for specific contexts [14,26]. For example, NDVI has been shown to saturate at high biomass (e.g., tropical rainforests) and be affected by canopy background, which is a concern in areas of low biomass [23]. The Enhanced Vegetation Index (EVI), which is more sensitive to canopy structural variations such as leaf area index (LAI), was developed to improve sensitivity in high biomass areas and reduce the influence of soil background and atmospheric effects [27].

In arid and semi-arid environments in particular, vegetation is generally sparse [28], and soil background can significantly affect spectral response [18]. Soil-adjusted indices have been developed to dissociate the background effects of soils from vegetation signals (e.g., [13,29]). An example is the Soil Adjusted Vegetation Index (SAVI), which extends NDVI by including an adjustment factor to account for soil background [23]. Alternatively, orthogonal indices, such as the Tasseled Cap (TC) transformation bands [30], have also been found to be less sensitive to the effects of soil background than other greenness indices [31]. As senescent vegetation and litter are common features of arid and semi-arid areas [18], indices that capture reflectance in the SWIR wavelengths have been useful for isolating dry vegetation signals from green vegetation and soil in these environments (e.g., [32,33]).

Several semi-arid woodland communities in south-eastern Australia have seen little to no regeneration of both their overstorey and many native understorey species in several decades, despite livestock removal and introduced herbivore control measures [34,35]. Western grey kangaroos are thought to switch from grass to other browse (e.g., shrub and tree seedlings) when grass biomass falls below 400 kg ha⁻¹ for sustained periods, which is likely to occur during dry summer and autumn months [36,37]. Managers are seeking an efficient, cost-effective way of obtaining seasonal understorey biomass estimates, particularly grass biomass, without the need for site visitation. Although empirical relationships between understorey biomass and remotely sensed VIs have been developed for several semi-arid areas around the world [18], these relationships are lacking for the semi-arid communities in this region. Furthermore, few studies assess the spatial and temporal transferability of biomass-VI relationships [18]. Understorey biomass information would allow managers to anticipate a drop in forage availability, thus triggering population control efforts to reduce the browsing risk to native understorey and tree seedlings as well as promote woodland regeneration.

In this study, we compared the ability of several remotely sensed vegetation indices to describe and predict total understorey (live and dead, all growth forms), live understorey (all growth forms), and grass biomass (live and dead, annual and perennial graminoids) in a semi-arid environment over a period of 2.5 years. We aimed to: (1) determine the most useful VIs to include in predictive models for understorey biomass, (2) examine whether models could be improved and extended to other sites when including additional soil moisture and vegetation variables, and (3) develop models appropriate for management that require no site visitation. A validation understorey biomass dataset was collected from

existing and new sites in the autumn following the main sampling period, and were used to test the predictive performance of the first two models.

2. Materials and Methods

2.1. Study Area

Field sites were located in the Pine Plains area of Wyperfeld National Park (NP), south-eastern Australia (Figure 1). Wyperfeld NP is semi-arid with a mean annual rainfall of 332 mm [38]. Over the sampling period, the region experienced both higher than average rainfall (404 mm in 2016 and 348 mm in 2017) and lower than average rainfall (143 mm in 2019) [38]. Rainfall occurs predominantly throughout winter and spring, with approximately 60% of mean annual precipitation falling between May and October [38].

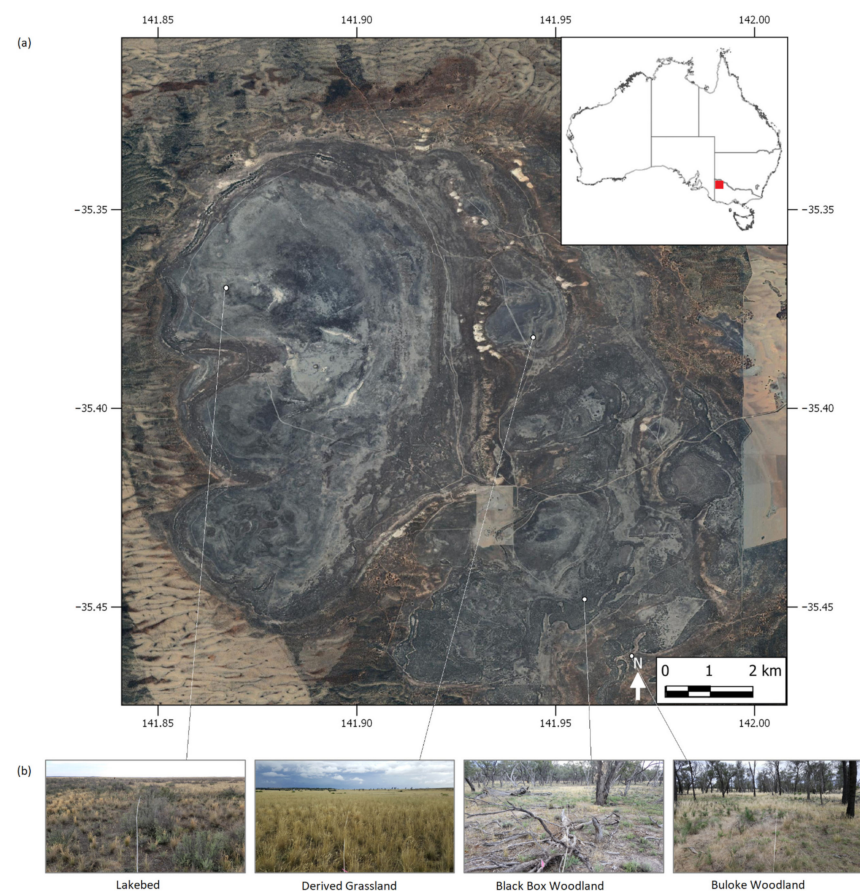


Figure 1. (a) Map of the Pine Plains area of Wyperfeld National Park, south-eastern Australia (inset, red square). The background image is a Google Satellite XYZ tile basemap; (b) Images captured in December (summer) 2017, which highlight the variation in structure and composition of the vegetation communities sampled.

The study area is largely a mosaic of woodland communities, dry lakebeds, and derived grasslands resulting from extensive historical clearing [39]. Woodlands are dominated by Buloke (*Allocasuarina luehmannii*, often co-dominated by Slender Cypress Pine (*Callitris gracilis* R.T.Baker)), Black Box (*Eucalyptus largiflorens* F.Muell.) or River Red Gum (*Eucalyptus camaldulensis* Dehnh.), with understories composed of grasses, forbs, and chenopod shrubs.

2.2. Field Data

We collected aboveground understory biomass, comprising graminoids, forbs, and shrubs, over six seasons between December 2016 and May 2018. We sampled a total of 40 sites within Buloke Woodland ($n = 10$), Black Box Woodland ($n = 10$), Derived Grassland

($n = 10$), and Lakebed ($n = 10$). For a more detailed description of field methods, see Riquelme et al. [37].

A 90 m \times 90 m area of homogeneous vegetation in terms of structure and cover was chosen for each site, corresponding to a 3 \times 3 Landsat pixel arrangement. Although sampling focused on the centre 30 m \times 30 m pixel, a larger area was selected to allow for any satellite or GPS positional errors [40]. Five quadrats (0.5 m \times 0.5 m each) were placed on the corners and middle of the central 30 m \times 30 m area. Within each quadrat, understorey biomass was clipped as closely to the ground as possible using grass shears, separated into live and dead, and placed into paper bags. Woody material was not clipped when sampling shrubs. Samples were dried at 70 °C for 72 h and then weighed.

We estimated grass biomass following the dry-weight-rank method developed by 't Mannetje and Haydock [41]: prior to clipping each quadrat, the top 3 understorey species in terms of dry weight were ranked visually. Dominant understorey species were classified into the following growth forms: annual graminoids, perennial graminoids, forbs, and shrubs. Grass biomass was calculated by multiplying the proportion of biomass classified as a graminoid by the total understorey dry weight [41].

An additional biomass dataset was collected in May 2019 and used as a validation dataset to test model performance over space and time. Of the 40 sites previously sampled, 24 were resampled to provide a temporal validation dataset. To enable spatial validation, 24 new sites were also sampled in this season. Sampling was distributed equally across vegetation types, with 12 (6 existing, 6 new) sites sampled within each. A total of 48 sites were surveyed in May 2019.

All data is available via the Open Science Framework [42].

2.3. Satellite Data

Landsat 7 Enhanced Thematic Mapper Plus (ETM+) and Landsat 8 Operational Land Imager (OLI) scenes spanning the sampling period were visually inspected for cloud cover. A scene was excluded if cloud was present over the study area. This could not be automated because although percentage cloud cover was included in the metadata, their spatial distribution throughout the scene was not specified. Surface reflectance (SR) and top-of-atmosphere (TOA) bands (path: 95, row: 85; Collection 1, Level 2) were downloaded from the United States Geological Survey (USGS) EROS Science Processing Architecture (ESPA) On Demand Interface [43]. NDVI, EVI, SAVI, MSAVI, and NDMI were calculated from SR data. TOA bands were required for the TC transformation, as transformation coefficients have only been developed for Landsat 8 TOA bands [44].

Although Landsat 7 and 8 broadly sample the same regions of the spectrum, systematic differences between sensors exist, particularly for TOA bands [45]. We adjusted Landsat 7 SR and TOA data to fit more closely with Landsat 8 data using coefficients derived for the Australian landscape [45].

Landsat satellites scan each scene with an 8-day interval; furthermore, approximately 40% of scans during the study period were deemed unusable due to cloud cover. To fill these temporal gaps and have remote sensing data that coincided with field surveys, a Generalised Additive Model (GAM) [46] was developed to model remote sensing data to daily values. GAMs were fitted using the mgcv package [47] in the R statistical environment [48]. GAMs were trained using 95 scenes between January 2016 and July 2019. The structure of the GAM was:

$$VI \sim s(\text{date}) + s(\text{date, by satellite}) + \text{tree cover} + \epsilon_i$$

where “date” denotes satellite scan date, “satellite” specifies Landsat 7 or 8 imagery, and “tree cover” refers to the probability of native tree cover at a given site [49]. A smoothing function (s) with a thin plate spline with shrinkage was applied to date in two ways: an average smooth for date (“s(date)”), as well as an individual smooth per satellite (“s(date, by satellite)”) to account for any deviations from the average smooth over time. Residual error is represented by ϵ_i .

The VIs (Table 1) were calculated using the RStoolbox package [50] in the R statistical environment [48]. For each VI, mean values for the centre pixel (30 m × 30 m) were extracted at each site.

Table 1. Vegetation indices used in this study.

Vegetation Index	Formula	References
Normalised Difference Vegetation Index (NDVI)	$(\text{NIR} - \text{Red}) / (\text{NIR} + \text{Red})$	[17]
Enhanced Vegetation Index (EVI)	$2.5 \times ((\text{NIR} - \text{Red}) / (\text{NIR} + 6 \times \text{Red} - 7.5 \times \text{Blue} + 1))$	[27]
Soil Adjusted Vegetation Index (SAVI)	$((\text{NIR} - \text{Red}) / (\text{NIR} + \text{Red} + \text{L})) \times (1 + 0.5)$	[23]
Modified Soil Adjusted Vegetation Index (MSAVI)	$(2 \times \text{NIR} + 1 - \sqrt{((2 \times \text{NIR} + 1)^2 - 8 \times (\text{NIR} - \text{Red})))} / 2$	[29]
Normalised Difference Moisture Index (NDMI)	$(\text{NIR} - \text{SWIR1}) / (\text{NIR} + \text{SWIR1})$	[15]
Tasseled Cap Brightness	$0.3029(\text{Blue}) + 0.2786(\text{Green}) + 0.4733(\text{Red}) + 0.5599(\text{NIR}) + 0.508(\text{SWIR1}) + 0.1872(\text{SWIR2})$	[30,44]
Tasseled Cap Greenness	$-0.2941(\text{Blue}) + -0.243(\text{Green}) + -0.5424(\text{Red}) + 0.7276(\text{NIR}) + 0.0713(\text{SWIR1}) + -0.1608(\text{SWIR2})$	[30,44]
Tasseled Cap Wetness	$0.1511(\text{Blue}) + 0.1973(\text{Green}) + 0.3283(\text{Red}) + 0.3407(\text{NIR}) + -0.7117(\text{SWIR1}) + -0.4559(\text{SWIR2})$	[30,44]

2.4. Analysis and Modelling

We used Generalised Linear Mixed Models (GLMMs) to test the ability of satellite-derived vegetation indices (alone or in combination) to describe and predict understorey biomass. Site was included as a random effect. A Pearson's correlation test was carried out on the VIs to determine the degree of correlation between indices. A pair that had a correlation coefficient $|r| > 0.7$ was considered to be highly correlated [51,52] and was therefore excluded from modelling. GLMMs were trained with biomass data collected in the field over 6 seasons between December 2016 and May 2018. GLMMs were fitted using the lme4 package [53] in the R statistical environment [48]. The general GLMM structure was:

$$\text{biomass} \sim \text{vegetation index} + \varepsilon_i$$

where "biomass" refers to biomass type (total understorey, live understorey, or grass) at a given site, and "vegetation index" represents a remote sensing vegetation index or combination of indices (additive). Residual site error is denoted by " ε_i ".

We then examined the Variance Inflation Factor (VIF) to determine the degree of collinearity among explanatory variables within each model [52,54]. Any variables with a VIF > 5 were excluded from the models. A model selection process was carried out for each biomass type. Models were ranked based on Akaike's Information Criterion (AIC) [55] and Akaike weight [56]. We also reported the marginal R^2 (R^2_m : the proportion of variance explained by the fixed effects only), the conditional R^2 (R^2_c : the proportion of variance explained by both the fixed and random effects) [57], and the degrees of freedom for each model. The model with the lowest AIC and highest weight for each biomass type was selected.

We also ran GLMMs with additional data on soil moisture [58], tree cover [49], and dominant understorey growth form (Table 2), to determine whether models could be further improved. Another model selection process was conducted, and the model with the lowest AIC and highest weight was selected for each biomass type.

Table 2. Additional explanatory variables used in models.

Variable	Resolution	Summary
Soil moisture	5 km × 5 km; Daily.	Root zone (top 1 m of soil profile) soil moisture obtained from the BoM Australian Landscape Water Balance (AWRA-L model) [58]. A mean soil moisture window of the previous month, with 2-week lag from clipping date, was chosen as it was most influential for understorey biomass in this study area [37].
Tree cover	22 m × 27 m approx.	Remotely sensed estimates of the probability of native tree cover [49].
Dominant understorey growth form	90 m × 90 m; Seasonal.	Growth forms were classified into annual graminoids, perennial graminoids, forbs, and shrubs. Dominant growth form was estimated at each site following the dry-weight-rank method [41].

We then used those models to develop models suitable for managers, who require a cost-efficient approach for estimating grass biomass seasonally, using only remotely sensed data. These incorporated all seasons' data (i.e., training and validation), but did not include additional data requiring field collection (i.e., dominant understorey growth form).

2.5. Model Validation

The predictive performance of the models was tested by predicting understorey biomass to autumn of the following year (May 2019), then comparing predictions to the observed understorey biomass data collected in the same season using Pearson's correlation test.

3. Results

3.1. Understorey Biomass

Mean values are reported with 95% confidence intervals. Total understorey biomass ranged from $835 \pm 41 \text{ kg ha}^{-1}$ (May (autumn) 2019) to $1324 \pm 100 \text{ kg ha}^{-1}$ (September (spring) 2017); live understorey biomass ranged between $84 \pm 15 \text{ kg ha}^{-1}$ (May (autumn) 2018) and $781 \pm 57 \text{ kg ha}^{-1}$ (July (winter) 2017), and grass biomass between $488 \pm 17 \text{ kg ha}^{-1}$ (autumn 2019) and $872 \pm 84 \text{ kg ha}^{-1}$ (September (spring) 2017) (Figure 2). Overall, summer and autumn were found to be seasons of lowest understorey biomass availability, with live understorey and grass biomass falling below the forage-switch threshold [36] for extended periods during those seasons (Figure 2).

Total understorey and grass biomass were significantly higher in open sites compared to woodland sites across all seasons (Figure 2). For live understorey biomass, this trend was only seen during winter and spring. Live biomass was similar across all vegetation types during the drier summer and autumn months (Figure 2). For more detail, refer to Riquelme et al. [37].

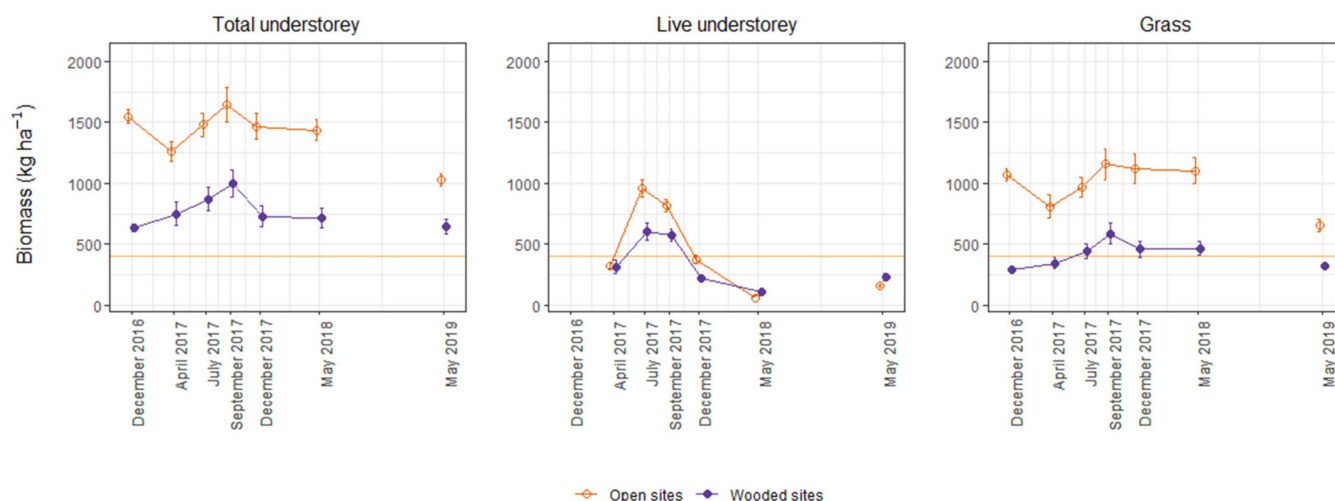


Figure 2. Mean understorey biomass for each sampling occasion in open and wooded sites, with 95% confidence intervals ($n = 40$, except May 2019 where $n = 48$). A validation dataset was collected in May 2019. Orange reference line represents purported forage-switch threshold (adapted from [36]).

3.2. Vegetation Indices

All VIs, except for brightness, followed a similar trend through time, though slopes tended to vary (Figure 3). VI values tended to peak in the wetter winter and spring months, which corresponded to winter seasons with average or above average rainfall (Figure 3) [38]. The opposite was generally true for brightness (Figure 3). As conditions gradually dried out over 2018–2019, values fell (again, except for brightness). Seasonal fluctuations also tended to flatten, which was seen for all VIs. VI values were similar across open and wooded sites during more mesic conditions, but diverged during drier years, with a more pronounced decrease in open sites than in woodland (Figure 3).

Most VIs, excluding brightness, were strongly positively correlated (Pearson's $r = 0.75$ – 0.99). In contrast, brightness had a high degree of negative correlation with wetness ($r = -0.74$) and a moderate negative correlation with NDVI ($r = -0.66$), but only weak negative correlations with all other indices ($r = -0.38$ – -0.45 ; Figure S1, Supplementary Materials).

3.3. Vegetation Index-Biomass Models

Explanatory power varied little between the top-ranked and lowest-ranked models for total understorey (mean difference in $R^2_m = 0.018$, and in $R^2_c = 0.024$) and grass biomass (mean difference in $R^2_m = 0.014$, and in $R^2_c = 0.019$) (Tables S1 and S3, Supplementary Materials). Models for live understorey biomass were more variable, however (mean difference in $R^2_m = 0.441$, and in $R^2_c = 0.583$) (Table S2, Supplementary Materials).

Brightness combined with MSAVI best explained live understorey biomass, and brightness and greenness accounted for the most variation in grass biomass (Table 3). Greenness alone best explained variation in total understorey biomass (Table 3), although the next-best model (brightness plus greenness) only had a difference in AIC of 3.62 (Table S1, Supplementary Materials).

Higher greenness values were associated with a modest increase in total understorey and grass biomass (Figure 4). Brightness was correlated with slightly lower grass biomass, but higher live understorey biomass (Figure 4). MSAVI also correlated with greater live biomass, although this was approximately twice the effect size of brightness (Figure 4).

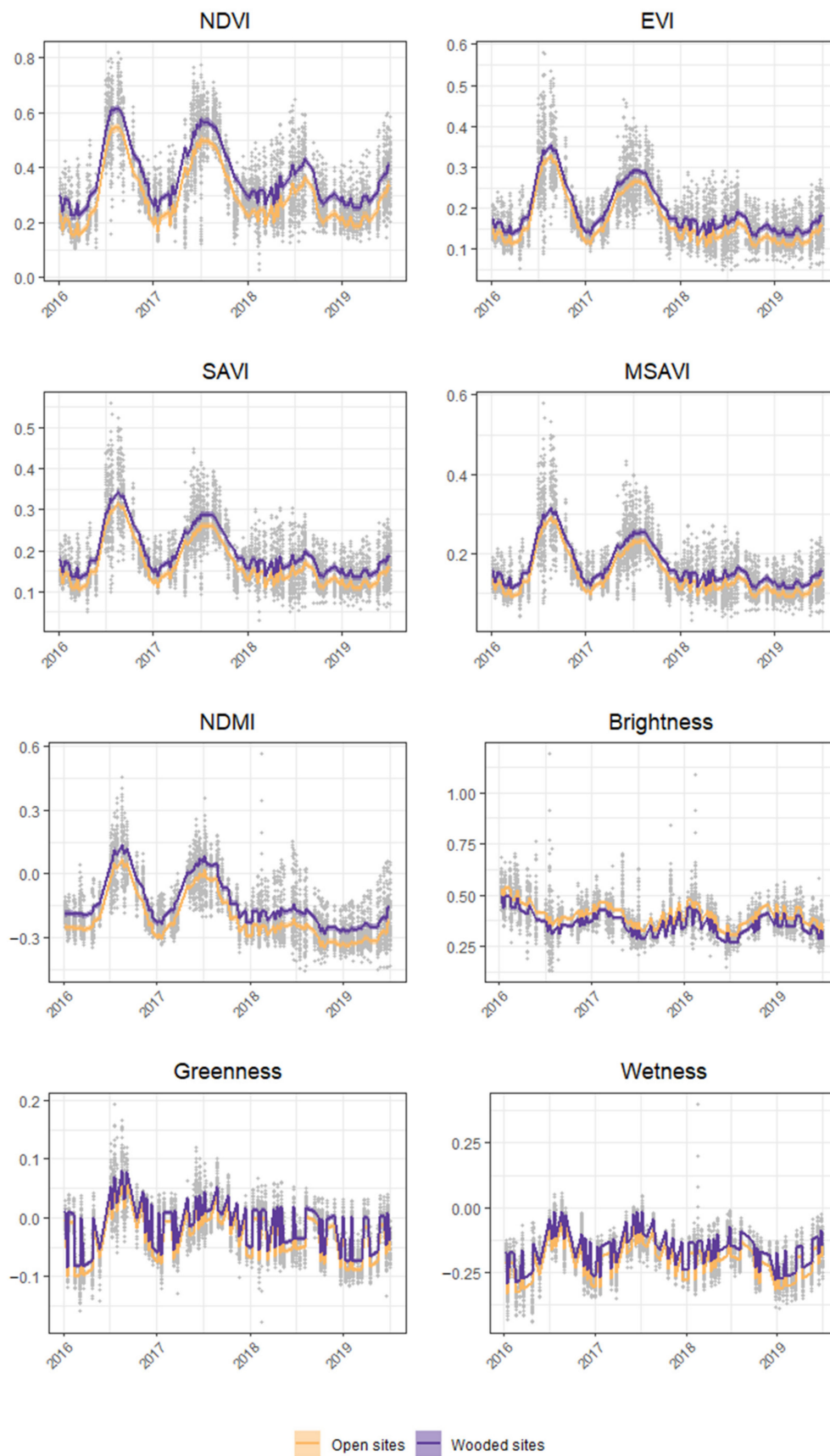
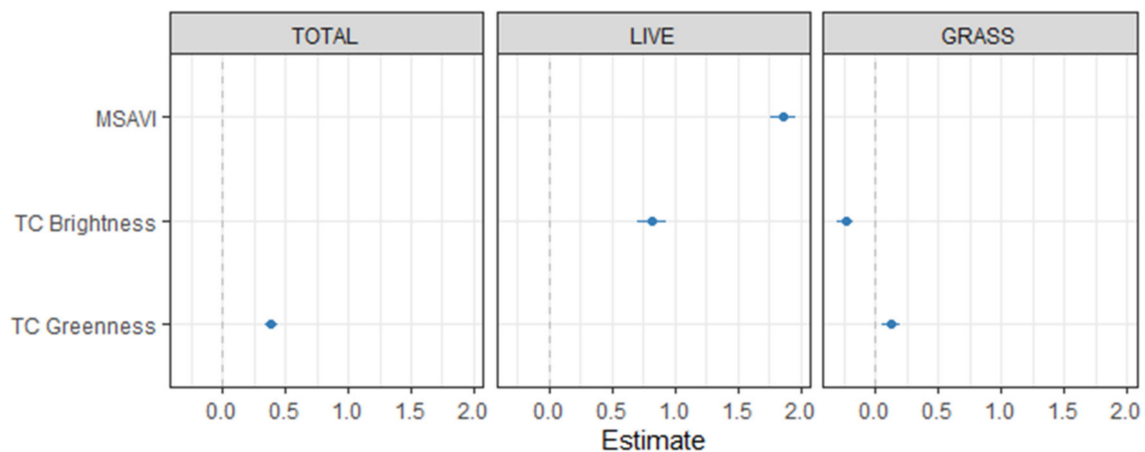


Figure 3. Mean vegetation index values for open vs. wooded sites over the study period. Lines represent GAM predictions, averaged for open and wooded sites, with 95% confidence intervals.

Table 3. Performance of top-ranked model for each understorey biomass type.

Model	R ² m	R ² c	t Value of Predictors
TOTAL ~ Greenness + ϵ_i	0.026	0.897	14.26
LIVE ~ Brightness + MSAVI + ϵ_i	0.441	0.715	14.16, 35.43
GRASS ~ Brightness + Greenness + ϵ_i	0.016	0.878	−7.64, 3.33

**Figure 4.** Effects plots for top model for each biomass type. Points denote effect sizes of explanatory variables and are shown with 95% confidence intervals. Blue represents a significant effect.

3.4. Vegetation Index-Biomass Models with Additional Variables

When adding soil moisture, tree cover, and dominant understorey growth form to the models, the top-performing model for live biomass included EVI instead of brightness and MSAVI (Table 4). The VIs in the top-performing total and grass biomass models remained unchanged. Performing a VIF test on the supplementary models only excluded certain live biomass models, though total and grass biomass models were again unaffected (Tables S4–S6, Supplementary Materials).

Table 4. Performance of top-ranked model (with additional variables) for each understorey biomass type. Dominant understorey growth form (Dom. G.F.) is a categorical variable, comprising annual graminoids, forbs, perennial graminoids, and shrubs.

Model	R ² m	R ² c	t Value of Predictors
TOTAL ~ Greenness + S.M. + Tree C. + Dom. G.F. + ϵ_i	0.428	0.881	12.78, −0.25, −6.89, 40.07, 38.66, 40.87, 39.61
LIVE ~ EVI + S.M. + Tree C. + Dom. G.F. + ϵ_i	0.602	0.746	3.34, 25.49, −3.40, 34.17, 33.67, 41.33, 37.15
GRASS ~ Brightness + Greenness + S.M. + Tree C. + Dom. G.F. + ϵ_i	0.483	0.890	−5.49, 5.03, −1.53, −7.01, 35.21, 26.26, 34.16, 29.73

Total and grass biomass models improved the most when including additional variables (compared to VI-only models) but only when excluding site effects: R²m improved by 0.402 for total biomass, and by 0.467 for grass biomass (Table 4). The live biomass model also improved, but less dramatically, with an increase in R²m of 0.161 (Table 4). There was little change in R²c for all biomass types when including extra explanatory variables (mean difference of 0.020; Table 4).

Tree cover showed a significant negative correlation with all understorey biomass types, especially for total and grass biomass; live biomass, on the other hand, was most strongly correlated to soil moisture (Figure 5). Dominant understorey growth form showed variable relationships with understorey biomass: live biomass was generally higher in sites

dominated by forbs or shrubs, and grass biomass was higher in sites dominated by annual graminoids (Figure 5). Growth form had no significant relationship with total understorey biomass, however (Figure 5).

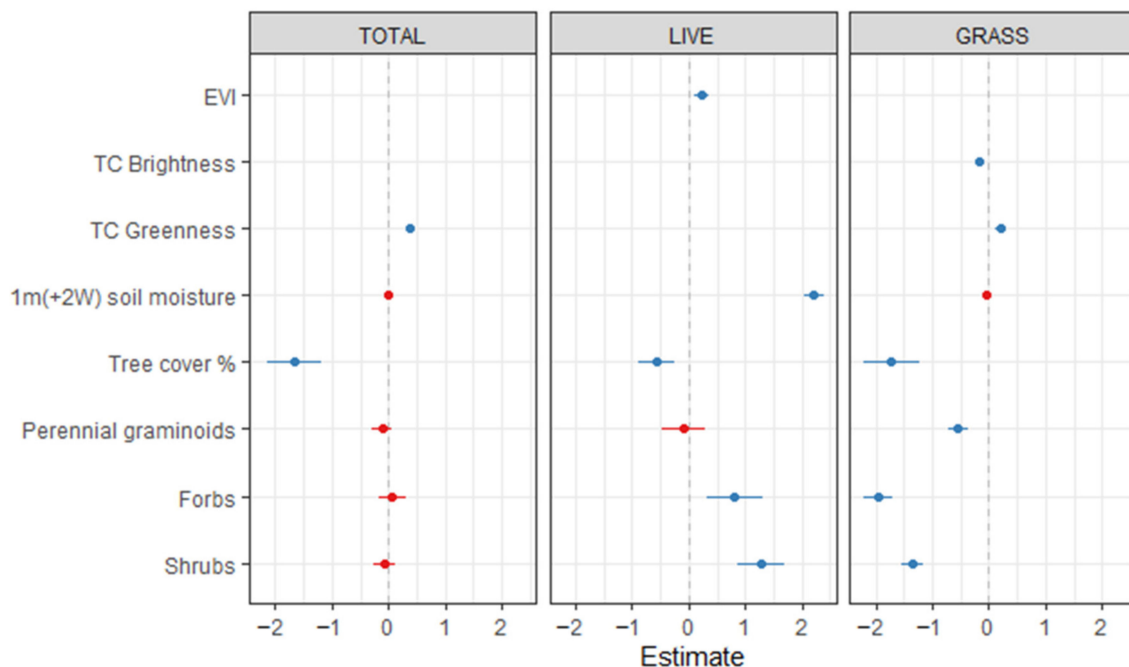


Figure 5. Effects plots for top model (with additional variables) for each understorey biomass type. Points denote effect sizes of explanatory variables and are shown with 95% confidence intervals. Blue represents a significant effect and red represents a non-significant effect.

3.5. Vegetation Index-Biomass Models for Management

Overall, the management models, which included soil moisture and tree cover but not dominant understorey growth form, performed better than VI-only models when modelling with only the main effects (mean improvement in R^2_m of 0.251; Table 5). In particular, R^2_m improved by 0.295 for total understorey biomass and by 0.296 for grass biomass (Table 5). The management model for live understorey biomass ($R^2_m = 0.443$, $R^2_c = 0.726$; Table 5) explained a similar amount of biomass as the live VI-only model (Table 3). Nevertheless, the management models did not account for as much variation in understorey biomass as the models with additional variables (Table 4), even when modelling with biomass data from all seasons (Table 5). The performance of all models was quite similar when modelling with site effects (Tables 3–5).

Table 5. Performance of top-ranked management model for each understorey biomass type (all data included).

Model	R^2_m	R^2_c	t Value of Predictors
TOTAL ~ Greenness + S.M. + Tree C. + ϵ_i	0.321	0.870	15.33, 0.44, -6.49
LIVE ~ EVI + S.M. + Tree C. + ϵ_i	0.443	0.726	2.70, 19.73, -1.30
GRASS ~ Brightness + Greenness + S.M. + Tree C. + ϵ_i	0.312	0.844	-4.65, 9.08, -0.16, -6.76

Management models with coefficients are presented in Table S7 (Supplementary Materials).

3.6. Model Validation

We tested the predictive performance of the models by comparing biomass predicted for May 2019 to observed biomass. Biomass was predicted by taking the random effects of

site into account (Figure 6, top row), as well as by considering only the main effects (i.e., vegetation indices; Figure 6, bottom row). Predicted understory biomass was more similar to observed values when modelling with site effects (Figure 6).

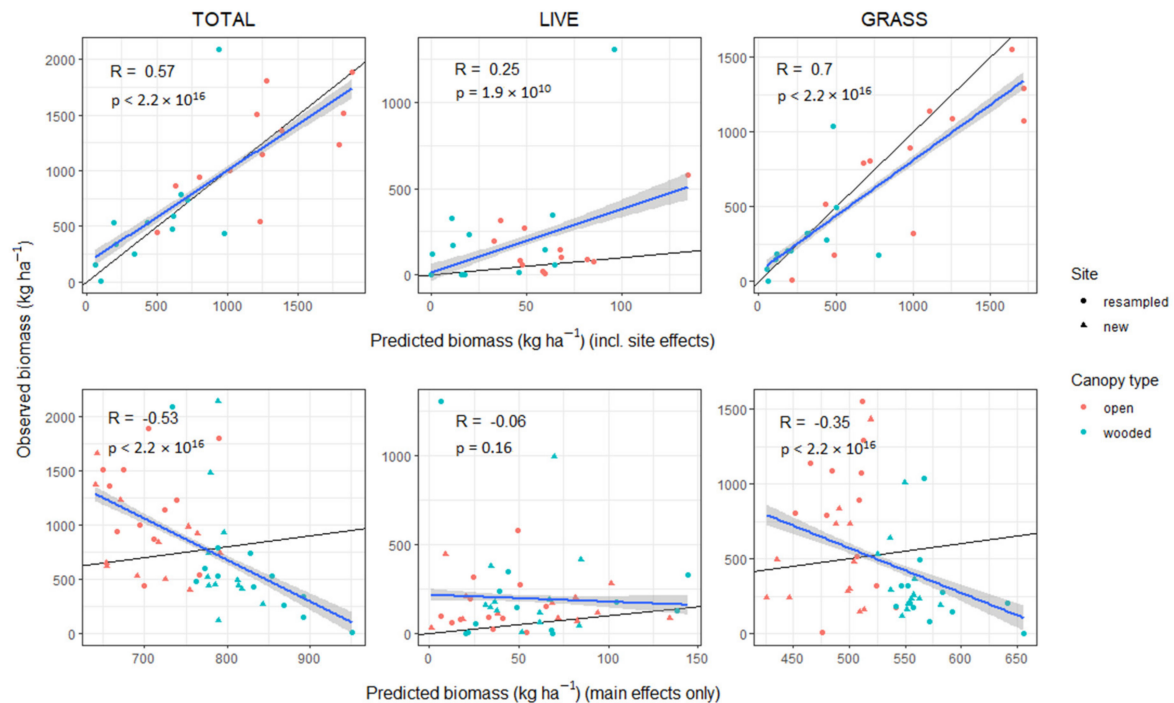


Figure 6. Validation plots for models with VIs only: total understory, live understory and grass biomass (predicted using main and site effects (**top** row), and using main effects only (**bottom** row)). Blue lines indicate the linear trend in correlation between predicted and observed values, with standard error represented by the grey ribbons. Black lines indicate a 1:1 relationship. Df = 622.

When including site effects, the model predicted 57% of total understory biomass (Figure 6). This was even higher for grass biomass (70%), although grass was generally overpredicted at sites with higher biomass (Figure 6). The model's predictive ability was lower for live understory biomass (25%; Figure 6). Live biomass was consistently underpredicted, especially as biomass increased, although a single outlier site exerted a large influence on patterns in the validation (Figure 6). In contrast, validation showed a low to moderate negative correlation with total understory and grass biomass, and almost no correlation with live understory biomass (Figure 6).

The predictive ability of the models' main effects improved when including soil moisture, tree cover, and dominant understory growth form: correlation between predicted and observed live biomass increased by 0.16, by 0.89 for total, and by 0.9 for grass biomass (Figure 7). Predictive ability when including site effects was little changed (Figure 7).

The management models were developed using all seasons' data (including validation dataset); hence, model validation was not carried out.

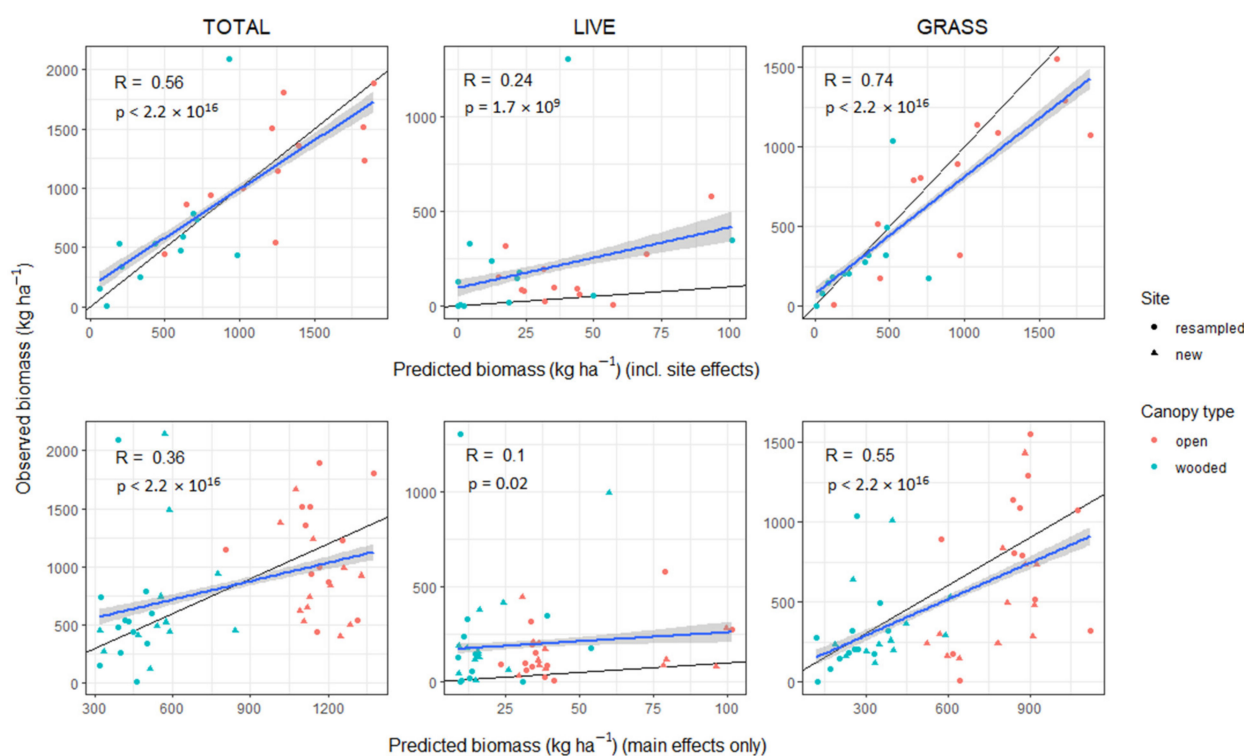


Figure 7. Validation plots for models with additional variables: total understorey, live understorey and grass biomass (predicted using main and site effects (**top** row), and using main effects only (**bottom** row)). Blue lines indicate the linear trend in correlation between predicted and observed values, with standard error represented by the grey ribbons. Black lines indicate a 1:1 relationship. Df = 622.

4. Discussion

4.1. Vegetation Index-Biomass Models

Remotely sensed VIs performed best for grass biomass, with 70% of variation accounted for when predicting to a new season in external validation, although VIs explained only 25% of variation in live understorey biomass. The ability of remote sensing to predict live biomass through time may be limited by the complex and dynamic relationships between biomass and remote sensing signals across seasons [59]. For example, the timing and intensity of rainfall events, which are highly variable in dry environments [60], can trigger species or growth-form specific phenological responses, thus impacting reflectance [9,61]. Moreover, grass and total understorey biomass included standing dead matter, which may have masked some of the reflectance of green vegetation, especially early in the growing season as new growth emerged [62]. Changes in soil moisture over time can alter soil brightness, which can also introduce noise into these relationships [63]. Soil signals are similar to those of dry vegetation [33]; this may also have affected the performance of VIs, especially in drier seasons.

While predictive performance of the models through time was mixed, VIs alone were unable to predict understorey biomass to new sites. Transferability of empirical models to new areas is one of the most significant challenges of biomass estimation using remote sensing [18]. Our results show that there is a clear effect of site on remote sensing signals. Site-specific relationships between biomass and reflectance have also been found elsewhere (e.g., [19,21,64]). The most obvious explanation for the failure to predict understorey biomass at new sites is that the VIs were unable to account for the confounding from the overstorey canopy. This can be seen in Figure 6, where wooded and open sites are predicted in the wrong order of biomass.

The lack of spatial transferability of the VI-only models can be explained in part by the fine-scale heterogeneity in topography and resource accumulation over the landscape,

which is characteristic of semi-arid areas [65]. The spatial resolution of the Landsat sensors was unlikely to be fine enough to capture this variation. Furthermore, as stated by Graetz [66], “all pixels are mixels”, in other words, that each pixel is an average of several landscape components, including vegetation, litter, soil, and shadows.

The influence of soil background and litter on reflectance was likely significant, especially during drier periods. The inclusion of the TC brightness index in the top models for live understorey and grass biomass indicated that it was a useful complement to greenness indices for explaining understorey biomass variation in the study area. Other studies in semi-arid regions have also highlighted the utility of brightness in biomass estimation (e.g., [20,67]).

Atmospheric effects are another source of noise in the signal, which can be more difficult to correct in heterogeneous landscapes [68]. Additionally, discrepancies between Landsat 7 and 8 sensors exist, particularly in top-of-atmosphere reflectance. This was also apparent in our results. While adjustments can be made to reduce these, differences will remain at the pixel-level [45].

VI-biomass model performance may also be improved by including observed VI values for the scan dates that correspond to field sampling, rather than VI values predicted from the GAMs. These GAMs could be further enhanced by including more scans to provide temporal repetition to account for scenes deemed unusable due to cloud cover.

4.2. Vegetation Index-Biomass Models with Additional Variables

The predictive ability of the VI-biomass models to new sites was greatly improved by including tree cover, soil moisture, and dominant understorey growth form. This was most evident for total understorey and grass biomass models with additional landscape variables, where there was an improvement of 90% in predictive ability to new sites in external validation. Soil moisture can affect soil brightness, with an increase in soil moisture resulting in lower brightness values [23,69]. The timing and amount of rainfall can also be a determinant in species composition, which along with vegetation structure, can influence the relationships between remote sensing signals and biomass [61,63].

Growth form composition data improved the models' predictive ability, although collection in the field is time-consuming and labour-intensive. Managers require seasonal estimates of understorey biomass without the need to carry out extra field work. The management models were trained using all seasons' data, which as expected, performed better than the main or the supplementary models when predicting through time. However, the management model performance was somewhat lower than the supplementary models for live understorey and grass biomass when predicting to new sites. This suggests that growth form may be an important factor to consider when estimating understorey biomass, though it is not as important as tree cover and soil moisture.

4.3. Vegetation Index-Biomass Models for Management

Although managers do not currently use the purported forage-switch threshold [36] to inform herbivore management, they are interested in incorporating it into management decision-making. As this threshold is based on grass biomass, the ability to reliably estimate grass biomass is particularly important in this context. The VI-biomass model, which did not include additional variables, was only useful at sites the model was trained on. Furthermore, it tended to overpredict grass at sites with high biomass. This means that this model may overestimate forage availability when in reality, it has fallen below the threshold, masking an increased browsing risk to seedlings. VIs were unable to predict understorey biomass to new sites without additional landscape scale variables. The performance of the management models demonstrates that by including remotely sensed soil moisture and tree cover data in the models, managers may better forecast forage availability across the study area without needing to collect field data.

5. Conclusions

Understorey biomass estimation is complex, and the choice of remote sensing variable, or combination of variables, is context-dependent [14,18]. Our results show that brightness is an important variable in this semi-arid environment and can improve the explanatory power of models with an index measuring vegetation greenness. However, VIs alone are not enough to predict biomass adequately, particularly to new sites. GLMMs could be further improved by the inclusion of herbivore density data specific to our sites, which were not available at the time of our study. As herbivore dynamics are complex, and their impacts on vegetation reflectance in this environment are unclear, further work to understand these relationships is needed. Finer spatial scale remote sensing data is required for improved biomass estimation in this heterogeneous environment, such as those obtained using unmanned aerial vehicles (UAVs). Although most remotely sensed biomass estimation studies have focused on optical data, there is also potential to integrate other data, such as Synthetic Aperture Radar (SAR) or Light Detection and Ranging (LIDAR) data, which have shown promising results in similar environments [70–72].

Supplementary Materials: The following supporting information can be downloaded at: <https://www.mdpi.com/article/10.3390/rs14102358/s1>, Figure S1: Matrix of vegetation index correlation coefficients; Table S1: Model outputs for vegetation index-total understorey biomass GLMMs (ϵ_i = residual error); Table S2: Model outputs for vegetation index-live understorey biomass GLMMs (ϵ_i = residual error); Table S3: Model outputs for vegetation index-grass biomass GLMMs (ϵ_i = residual error); Table S4: Model outputs for vegetation index-total understorey biomass GLMMs with additional variables (S.M. = soil moisture (1-month window + 2-week lag), Tree C. = percentage tree cover, Dom. G.F. = dominant understorey growth form, ϵ_i = residual error); Table S5: Model outputs for vegetation index-live understorey biomass GLMMs with additional variables (S.M. = soil moisture (1-month window + 2-week lag), Tree C. = percentage tree cover, Dom. G.F. = dominant understorey growth form, ϵ_i = residual error); Table S6: Model outputs for vegetation index-grass biomass GLMMs with additional variables (S.M. = soil moisture (1-month window + 2-week lag), Tree C. = percentage tree cover, Dom. G.F. = dominant understorey growth form, ϵ_i = residual error); Table S7: Management models with coefficients. GLMMs trained using all seasons' (training and validation) data.

Author Contributions: Conceptualization, L.R. (Linda Riquelme), D.H.D., L.R. (Libby Rumpff) and P.A.V.; methodology, L.R. (Linda Riquelme), D.H.D., L.R. (Libby Rumpff) and P.A.V.; software, L.R. (Linda Riquelme); validation, L.R. (Linda Riquelme), D.H.D., L.R. (Libby Rumpff) and P.A.V.; formal analysis, L.R. (Linda Riquelme), D.H.D., L.R. (Libby Rumpff) and P.A.V.; investigation, L.R. (Linda Riquelme), D.H.D., L.R. (Libby Rumpff) and P.A.V.; resources, P.A.V. and L.R. (Linda Riquelme); data curation, L.R. (Linda Riquelme); writing—original draft preparation, L.R. (Linda Riquelme); writing—review and editing, D.H.D., L.R. (Libby Rumpff) and P.A.V.; visualization, L.R. (Linda Riquelme); supervision, D.H.D., L.R. (Libby Rumpff) and P.A.V.; project administration, L.R. (Linda Riquelme), D.H.D., L.R. (Libby Rumpff) and P.A.V.; funding acquisition, P.A.V. and L.R. (Linda Riquelme). All authors have read and agreed to the published version of the manuscript.

Funding: This study was funded by the Parks Victoria Research Partners Panel, the Australian Government's National Environmental Science Programme through the Threatened Species Recovery Hub Project 1.2.2 Adaptive management of endangered Buloke woodlands, the Holsworth Wildlife Research Endowment (Ecological Society of Australia), the David H. Ashton Scholarship (University of Melbourne Botany Foundation), and the Bill Borthwick Student Scholarship (Victorian Environmental Assessment Council).

Data Availability Statement: The data that support this study are available via an Open Science Framework repository at doi: 10.17605/OSF.IO/GHQTC [42].

Acknowledgments: The authors are grateful to Jian Yen for his support in the development and visualisation of the GAMs. The authors would also like to thank our field assistants, especially Ami Bennett, Khorloo Batpurev, Manisha Bhardwaj, Louise O'Connor, David Uribe-Rivera, Alejandro Garza-García, and Emily Baldwin, as well as Matt Baker (Parks Victoria) for support in the field.

Conflicts of Interest: The authors declare no conflict of interest.

References

1. Keane, R.E.; Burgan, R.; van Wagten, J. Mapping Wildland Fuels for Fire Management across Multiple Scales: Integrating Remote Sensing, GIS, and Biophysical Modeling. *Int. J. Wildland Fire* **2001**, *10*, 301–309. [[CrossRef](#)]
2. Kerr, J.T.; Ostrovsky, M. From Space to Species: Ecological Applications for Remote Sensing. *Trends Ecol. Evol.* **2003**, *18*, 299–305. [[CrossRef](#)]
3. Wingate, V.R.; Phinn, S.R.; Kuhn, N.; Scarth, P. Estimating Aboveground Woody Biomass Change in Kalahari Woodland: Combining Field, Radar, and Optical Data Sets. *Int. J. Remote Sens.* **2018**, *39*, 577–606. [[CrossRef](#)]
4. Ballesteros, R.; Ortega, J.F.; Hernandez, D.; del Campo, A.; Moreno, M.A. Combined Use of Agro-Climatic and Very High-Resolution Remote Sensing Information for Crop Monitoring. *Int. J. Appl. Earth Obs. Geoinf.* **2018**, *72*, 66–75. [[CrossRef](#)]
5. Flombaum, P.; Sala, O.E. A Non-Destructive and Rapid Method to Estimate Biomass and Aboveground Net Primary Production in Arid Environments. *J. Arid Environ.* **2007**, *69*, 352–358. [[CrossRef](#)]
6. Michez, A.; Lejeune, P.; Bauwens, S.; Herinaina, A.; Blaise, Y.; Castro Muñoz, E.; Lebeau, F.; Bindelle, J. Mapping and Monitoring of Biomass and Grazing in Pasture with an Unmanned Aerial System. *Remote Sens.* **2019**, *11*, 473. [[CrossRef](#)]
7. Sinda-González, I.; Gil-Docampo, M.; Arza-García, M.; Grefa-Sánchez, J.; Yáñez-Simba, D.; Pérez-Guerrero, P.; Abril-Porras, V. Biomass Estimation of Pasture Plots with Multitemporal UAV-Based Photogrammetric Surveys. *Int. J. Appl. Earth Obs. Geoinf.* **2021**, *101*, 102355. [[CrossRef](#)]
8. Walton, K.M.; Spalinger, D.E.; Harris, N.R.; Collins, W.B.; Willacker, J.J. High Spatial Resolution Vegetation Mapping for Assessment of Wildlife Habitat: Mapping for Assessment of Wildlife Habitat. *Wildl. Soc. Bull.* **2013**, *37*, 906–915. [[CrossRef](#)]
9. Garrouette, E.; Hansen, A.; Lawrence, R. Using NDVI and EVI to Map Spatiotemporal Variation in the Biomass and Quality of Forage for Migratory Elk in the Greater Yellowstone Ecosystem. *Remote Sens.* **2016**, *8*, 404. [[CrossRef](#)]
10. Palmer, A.R.; Samuels, I.; Cupido, C.; Finca, A.; Kangombe, W.F.; Yunusa, I.A.; Vetter, S.; Mapaure, I. Aboveground Biomass Production of a Semi-Arid Southern African Savanna: Towards a New Model. *Afr. J. Range Forage Sci.* **2016**, *33*, 43–51. [[CrossRef](#)]
11. Doan, T.; Guo, X. Understanding Bison Carrying Capacity Estimation in Northern Great Plains Using Remote Sensing and GIS. *Can. J. Remote Sens.* **2019**, *45*, 139–162. [[CrossRef](#)]
12. Raab, C.; Riesch, F.; Tonn, B.; Barrett, B.; Meißner, M.; Balkenhol, N.; Isselstein, J. Target-oriented Habitat and Wildlife Management: Estimating Forage Quantity and Quality of Semi-natural Grasslands with Sentinel-1 and Sentinel-2 Data. *Remote Sens. Ecol. Conserv.* **2020**, *6*, 381–398. [[CrossRef](#)]
13. Baret, F.; Guyot, G.; Major, D.J. TSAVI: A Vegetation Index Which Minimizes Soil Brightness Effects On LAI And APAR Estimation. In Proceedings of the 12th Canadian Symposium on Remote Sensing Geoscience and Remote Sensing Symposium, Vancouver, BC, Canada, 10–14 July 1989; IEEE: Vancouver, Canada, 1989; Volume 3, pp. 1355–1358.
14. Bannari, A.; Morin, D.; Bonn, F.; Huete, A.R. A Review of Vegetation Indices. *Remote Sens. Rev.* **1995**, *13*, 95–120. [[CrossRef](#)]
15. Hardisky, M.A.; Klemas, V.; Smart, R.M. The Influence of Soil Salinity, Growth Form, and Leaf Moisture on the Spectral Radiance of *Spartina Alterniflora* Canopies. *Photogramm. Eng. Remote Sens.* **1983**, *49*, 77–83.
16. Huete, A.R.; Liu, H.Q.; Batchily, K.; van Leeuwen, W. A Comparison of Vegetation Indices over a Global Set of TM Images for EOS-MODIS. *Remote Sens. Environ.* **1997**, *59*, 440–451. [[CrossRef](#)]
17. Rouse, J.W.; Haas, R.H.; Schell, J.A.; Deering, D.W.; Harlan, J.C. *Monitoring the Vernal Advancement and Retrogradation (Greenwave Effect) of Natural Vegetation*; Texas A&M University Remote Sensing Center: College Station, TX, USA, 1974.
18. Eisfelder, C.; Kuenzer, C.; Dech, S. Derivation of Biomass Information for Semi-Arid Areas Using Remote-Sensing Data. *Int. J. Remote Sens.* **2012**, *33*, 2937–2984. [[CrossRef](#)]
19. Foody, G.M.; Boyd, D.S.; Cutler, M.E.J. Predictive Relations of Tropical Forest Biomass from Landsat TM Data and Their Transferability between Regions. *Remote Sens. Environ.* **2003**, *85*, 463–474. [[CrossRef](#)]
20. Samimi, C.; Kraus, T. Biomass Estimation Using Landsat-TM and -ETM+. Towards a Regional Model for Southern Africa? *GeoJournal* **2004**, *59*, 177–187. [[CrossRef](#)]
21. Wessels, K.J.; Prince, S.D.; Zambatis, N.; MacFadyen, S.; Frost, P.E.; Van Zyl, D. Relationship between Herbaceous Biomass and 1-km² Advanced Very High Resolution Radiometer (AVHRR) NDVI in Kruger National Park, South Africa. *Int. J. Remote Sens.* **2006**, *27*, 951–973. [[CrossRef](#)]
22. Cho, M.A.; Skidmore, A.K. Hyperspectral Predictors for Monitoring Biomass Production in Mediterranean Mountain Grasslands: Majella National Park, Italy. *Int. J. Remote Sens.* **2009**, *30*, 499–515. [[CrossRef](#)]
23. Huete, A.R. A Soil-Adjusted Vegetation Index (SAVI). *Remote Sens. Environ.* **1988**, *25*, 295–309. [[CrossRef](#)]
24. Lewis, M. Spectral Characterization of Australian Arid Zone Plants. *Can. J. Remote Sens.* **2002**, *28*, 219–230. [[CrossRef](#)]
25. Kaufman, Y.J.; Tanre, D. Atmospherically Resistant Vegetation Index (ARVI) for EOS-MODIS. *IEEE Trans. Geosci. Remote Sens.* **1992**, *30*, 261–270. [[CrossRef](#)]
26. Silleos, N.G.; Alexandridis, T.K.; Gitas, I.Z.; Perakis, K. Vegetation Indices: Advances Made in Biomass Estimation and Vegetation Monitoring in the Last 30 Years. *Geocarto Int.* **2006**, *21*, 21–28. [[CrossRef](#)]
27. Huete, A.; Didan, K.; Miura, T.; Rodriguez, E.P.; Gao, X.; Ferreira, L.G. Overview of the Radiometric and Biophysical Performance of the MODIS Vegetation Indices. *Remote Sens. Environ.* **2002**, *83*, 195–213. [[CrossRef](#)]
28. Chen, Y.; Gillieson, D. Evaluation of Landsat TM Vegetation Indices for Estimating Vegetation Cover on Semi-Arid Rangelands: A Case Study from Australia. *Can. J. Remote Sens.* **2009**, *35*, 435–446. [[CrossRef](#)]

29. Qi, J.; Kerr, Y.; Chehbouni, A. External Factor Consideration in Vegetation Index Development. In Proceedings of the CNES, Proceedings of 6th International Symposium on Physical Measurements and Signatures in Remote Sensing, Val D'Isere, France, 17–22 January 1994.
30. Kauth, R.J.; Thomas, G.S. The Tasseled Cap—A Graphic Description of the Spectral-Temporal Development of Agricultural Crops as Seen by LANDSAT. In Proceedings of the Symposium on Machine Processing of Remotely Sensed Data; Purdue University: West Lafayette, IN, USA, 1976; p. 13.
31. Huete, A.R.; Jackson, R.D.; Post, D.F. Spectral Response of a Plant Canopy with Different Soil Backgrounds. *Remote Sens. Environ.* **1985**, *17*, 37–53. [[CrossRef](#)]
32. Qi, J.; Marsett, R.C.; Heilman, P. Rangeland Vegetation Cover Estimation from Remotely Sensed Data. In Proceedings of the 2nd International Conference on Geospatial Information in Agriculture and Forestry, Lake Buena Vista, FL, USA, 10–12 January 2000.
33. Jacques, D.C.; Kergoat, L.; Hiernaux, P.; Mougin, E.; Defourny, P. Monitoring Dry Vegetation Masses in Semi-Arid Areas with MODIS SWIR Bands. *Remote Sens. Environ.* **2014**, *153*, 40–49. [[CrossRef](#)]
34. Cheal, D. A Park with a Kangaroo Problem. *Oryx* **1986**, *20*, 95–99. [[CrossRef](#)]
35. Taylor, L.; Pegler, P. *Total Grazing Management Plan for the Restoration of Semi-Arid Woodland and Floodplain Vegetation Communities in North-Western (Mallee) Parks 2016–2021*; State Government of Victoria: Melbourne, VIC, Australia, 2016.
36. Norbury, G.L. Diet Selection and Demography of the Western Grey Kangaroo: *Macropus Fuliginosus Melanops Desmarest* in Hattah-Kulkyne National Park, Victoria. Ph.D. Thesis, Monash University, Clayton, VIC, Australia, 1987.
37. Riquelme, L.; Rumpff, L.; Duncan, D.H.; Vesk, P.A. Understanding the Spatiotemporal Dynamics of Understorey Biomass in Semi-Arid Woodlands of South-Eastern Australia. *Rangel. J.* **2022**, *44*, 47–59. [[CrossRef](#)]
38. Bureau of Meteorology Monthly Rainfall–076065–Bureau of Meteorology. Available online: http://www.bom.gov.au/jsp/ncc/cdio/weatherData/av?p_nccObsCode=139&p_display_type=dataFile&p_startYear=&p_c=&p_stn_num=076065 (accessed on 27 March 2022).
39. Miller, J.; Gibson, M.; Westbrooke, M.; Wilcock, P.; Brown, G. *Condition of Vegetation in the Riverine Woodlands of Wyperfeld National Park*; Centre for Environmental Management, University of Ballarat: Ballarat, VIC, Australia, 1998.
40. Reinke, K.; Jones, S. Integrating Vegetation Field Surveys with Remotely Sensed Data. *Ecol. Manag. Restor.* **2006**, *7*, S18–S23. [[CrossRef](#)]
41. 't Mannetje, L.; Haydock, K.P. The Dry-Weight-Rank Method for the Botanical Analysis of Pasture. *Grass Forage Sci.* **1963**, *18*, 268–275. [[CrossRef](#)]
42. Riquelme, L.; Rumpff, L.; Duncan, D.H.; Vesk, P.A. OSF|Biom_data.csv. Available online: <https://osf.io/4kg6d/> (accessed on 25 November 2021).
43. United States Geological Survey ESPA—LSRD. Available online: <https://espa.cr.usgs.gov/> (accessed on 27 March 2022).
44. Baig, M.H.A.; Zhang, L.; Shuai, T.; Tong, Q. Derivation of a Tasseled Cap Transformation Based on Landsat 8 At-Satellite Reflectance. *Remote Sens. Lett.* **2014**, *5*, 423–431. [[CrossRef](#)]
45. Flood, N. Continuity of Reflectance Data between Landsat-7 ETM+ and Landsat-8 OLI, for Both Top-of-Atmosphere and Surface Reflectance: A Study in the Australian Landscape. *Remote Sens.* **2014**, *6*, 7952–7970. [[CrossRef](#)]
46. Hastie, T.; Tibshirani, R. Generalized Additive Models. *Stat. Sci.* **1986**, *1*, 297–318. [[CrossRef](#)]
47. Wood, S.N. Fast Stable Restricted Maximum Likelihood and Marginal Likelihood Estimation of Semiparametric Generalized Linear Models: Estimation of Semiparametric Generalized Linear Models. *J. R. Stat. Soc. Ser. B* **2011**, *73*, 3–36. [[CrossRef](#)]
48. R Core Team. *R: A Language and Environment for Statistical Computing*; R Foundation for Statistical Computing: Vienna, Austria, 2020.
49. White, M.; Griffioen, P.; Newell, G. *Multi-Temporal Land Cover and Native Vegetation Extent for Victoria*; Technical Report No. 311; Department of Environment, Land, Water and Planning, Arthur Rylah Institute for Environmental Research: Heidelberg, VIC, Australia, 2020; p. 29.
50. Leutner, B.; Horning, N.; Schwalb-Willman, J. RStoolbox: Tools for Remote Sensing Data Analysis. R package version 0.2.6. 2019. Available online: <https://CRAN.R-project.org/package=RStoolbox> (accessed on 25 November 2021).
51. Asuero, A.G.; Sayago, A.; González, A.G. The Correlation Coefficient: An Overview. *Crit. Rev. Anal. Chem.* **2006**, *36*, 41–59. [[CrossRef](#)]
52. Dormann, C.F.; Elith, J.; Bacher, S.; Buchmann, C.; Carl, G.; Carré, G.; Marquéz, J.R.G.; Gruber, B.; Lafourcade, B.; Leitão, P.J.; et al. Collinearity: A Review of Methods to Deal with It and a Simulation Study Evaluating Their Performance. *Ecography* **2013**, *36*, 27–46. [[CrossRef](#)]
53. Bates, D.; Mächler, M.; Bolker, B.; Walker, S. Fitting Linear Mixed-Effects Models Using lme4. *J. Stat. Softw.* **2015**, *67*, 1–48. [[CrossRef](#)]
54. Logan, M. *Biostatistical Design and Analysis Using R: A Practical Guide*, 1st ed.; Wiley: Hoboken, NJ, USA, 2010; ISBN 9781405190084.
55. Akaike, H. Information Theory and an Extension of the Maximum Likelihood Principle. In *Proceeding of the Second International Symposium on Information Theory, Tsahkadsor, Armenia, 2–8 September 1971*; Akademiai Kiado: Budapest, Hungary, 1973; pp. 267–281.
56. Burnham, K.P.; Anderson, D.R. *Model Selection and Multimodel Inference: A Practical Information-Theoretic Approach*, 2nd ed.; Springer-Verlag: New York, NY, USA, 2002; ISBN 9780387953649.
57. Nakagawa, S.; Schielzeth, H. A General and Simple Method for Obtaining R² from Generalized Linear Mixed-Effects Models. *Methods Ecol. Evol.* **2013**, *4*, 133–142. [[CrossRef](#)]

58. Bureau of Meteorology Australian Landscape Water Balance. Available online: <http://www.bom.gov.au/water/landscape/#/sm/Actual/day/> (accessed on 5 February 2020).
59. Diouf, A.; Lambin, E.F. Monitoring Land-Cover Changes in Semi-Arid Regions: Remote Sensing Data and Field Observations in the Ferlo, Senegal. *J. Arid Environ.* **2001**, *48*, 129–148. [[CrossRef](#)]
60. Nano, C.E.M.; Pavey, C.R. Refining the ‘Pulse-Reserve’ Model for Arid Central Australia: Seasonal Rainfall, Soil Moisture and Plant Productivity in Sand Ridge and Stony Plain Habitats of the Simpson Desert. *Austral Ecol.* **2013**, *38*, 741–753. [[CrossRef](#)]
61. Ustin, S.L.; Gamon, J.A. Remote Sensing of Plant Functional Types. *New Phytol.* **2010**, *186*, 795–816. [[CrossRef](#)]
62. Wehlage, D.; Gamon, J.; Thayer, D.; Hildebrand, D. Interannual Variability in Dry Mixed-Grass Prairie Yield: A Comparison of MODIS, SPOT, and Field Measurements. *Remote Sens.* **2016**, *8*, 872. [[CrossRef](#)]
63. Mbow, C.; Fensholt, R.; Rasmussen, K.; Diop, D. Can Vegetation Productivity Be Derived from Greenness in a Semi-Arid Environment? Evidence from Ground-Based Measurements. *J. Arid Environ.* **2013**, *97*, 56–65. [[CrossRef](#)]
64. Huete, A.; Justice, C.; Liu, H. Development of Vegetation and Soil Indices for MODIS-EOS. *Remote Sens. Environ.* **1994**, *49*, 224–234. [[CrossRef](#)]
65. Tongway, D.J.; Ludwig, J.A. Small-Scale Resource Heterogeneity in Semi-Arid Landscapes. *Pac. Conserv. Biol.* **1994**, *1*, 201–208. [[CrossRef](#)]
66. Graetz, R.D. Satellite Remote Sensing of Australian Rangelands. *Remote Sens. Environ.* **1987**, *23*, 313–331. [[CrossRef](#)]
67. Moleele, N.; Ringrose, S.; Arnberg, W.; Lunden, B.; Vanderpost, C. Assessment of Vegetation Indexes Useful for Browse (Forage) Prediction in Semi-Arid Rangelands. *Int. J. Remote Sens.* **2001**, *22*, 741–756. [[CrossRef](#)]
68. Vermote, E.; Justice, C.; Claverie, M.; Franch, B. Preliminary Analysis of the Performance of the Landsat 8/OLI Land Surface Reflectance Product. *Remote Sens. Environ.* **2016**, *185*, 46–56. [[CrossRef](#)]
69. Todd, S.W.; Hoffer, R.M.; Milchunas, D.G. Biomass Estimation on Grazed and Ungrazed Rangelands Using Spectral Indices. *Int. J. Remote Sens.* **1998**, *19*, 427–438. [[CrossRef](#)]
70. Svoray, T.; Shoshany, M. SAR-Based Estimation of Areal Aboveground Biomass (AAB) of Herbaceous Vegetation in the Semi-Arid Zone: A Modification of the Water-Cloud Model. *Int. J. Remote Sens.* **2002**, *23*, 4089–4100. [[CrossRef](#)]
71. Li, A.; Dhakal, S.; Glenn, N.; Spaete, L.; Shinneman, D.; Pilliod, D.; Arkle, R.; McIlroy, S. Lidar Aboveground Vegetation Biomass Estimates in Shrublands: Prediction, Uncertainties and Application to Coarser Scales. *Remote Sens.* **2017**, *9*, 903. [[CrossRef](#)]
72. Anderson, K.E.; Glenn, N.F.; Spaete, L.P.; Shinneman, D.J.; Pilliod, D.S.; Arkle, R.S.; McIlroy, S.K.; Derryberry, D.R. Estimating Vegetation Biomass and Cover across Large Plots in Shrub and Grass Dominated Drylands Using Terrestrial Lidar and Machine Learning. *Ecol. Indic.* **2018**, *84*, 793–802. [[CrossRef](#)]